

## Nuclear interactions at volume reflection: Perturbative treatment

M. V. Bondarenco\*

*Kharkov Institute of Physics and Technology, 1 Academic Street, 61108 Kharkov, Ukraine*  
(Received 1 September 2011; published 22 March 2012)

Excess of nuclear interaction probability at volume reflection is evaluated within the approximation of dominance of the continuous planar potential and thin nuclear concentrations. The domain of the adopted approximations is determined. An estimate of the volume capture probability is provided. The theoretical predictions for inelastic nuclear interaction probability and for the final beam divergence are compared with the results of recent experiments, with satisfactory agreement within the theory applicability domain.

DOI: [10.1103/PhysRevSTAB.15.032802](https://doi.org/10.1103/PhysRevSTAB.15.032802)

PACS numbers: 61.85.+p, 29.27.-a, 45.10.-b

### I. INTRODUCTION

Volume reflection [1] of ultrarelativistic charged particles from curved atomic planes of an oriented bent crystal has proved to be a viable option for beam steering at high-energy particle accelerators [2–5]. The physical condition of its applicability essentially coincides with the Tsyganov condition for channeled beam deflection in a bent crystal:  $R > R_c$ , with  $R$  the crystal bending radius, and  $R_c$  the so-called critical radius proportional to the particle energy [Eq. (4) below]. In contrast to channeling, however, at volume reflection the particle passes through the crystal in an overbarrier mode, somewhere within the crystal volume finding a point (or a relatively small region) from which it reflects to the side opposite to that of the crystal bending. The advantages of the volume reflection mechanism are the large angular acceptance (equal to the crystal total bending angle), and almost 100% deflection efficiency. The price to pay is that volume reflection angle is of the order of the Lindhard's critical angle  $\theta_c = \sqrt{2V_0/E}$ , where  $V_0$  is the interplanar continuous potential well depth, and  $E$  the particle energy, so at  $E \gg V_0$  the angle of single deflection is pretty small. Fortunately, this difficulty can be surmounted by transmitting the particle through a sequence of bent crystals [6], or arranging a composite volume reflection from several crystallographic planes within one crystal [7], thereby multiplying the deflection angle. Experiments on volume reflection begun within a decade, and are currently continuing.

The theory of volume reflection is less mature than that for channeling. The physical origin of the reflection effect in a bent crystal is understood to be due to the asymmetry of the continuous potential in the area where the angles of atomic plane crossing by the particle become comparable to  $\theta_c$ . Particle dynamics in the pure continuous potential of

a uniformly bent crystal can be relatively easily calculated analytically, and the reflected beam angular distribution be evaluated as a function of the beam energy and the crystal bending radius [8,9].

In a real crystal, however, one must also take into account incoherent Coulomb scattering on individual atomic nuclei at close interactions with them. The condition for the incoherent scattering not to blur the beam deflection is the smallness of the multiple Coulomb scattering rms angle accumulated along the whole traversed crystal compared to the mean volume reflection angle. That still permits the usage of crystals with thickness by an order of magnitude exceeding the essential volume reflection region extent. However, in other respects, for instance for evaluation of the outgoing beam angular dispersion, the account of multiple Coulomb scattering is mandatory, and for volume capture treatment it is crucial.

It is worth mentioning that, besides elastic scattering at particle passage close to an atomic nucleus, nuclear interactions can also be inelastic, when the proton hits a nucleus directly. Inelastic interactions at high energy typically lead to multiple hadron production, which can be registered downstream in so-called beam loss monitors [10]. Since the rates of inelastic and close (incoherent) elastic events are proportional, by this method the relative rate of nuclear interactions can be directly measured [11].

For a rigorous treatment of incoherent multiple scattering at volume reflection, one needs to solve the corresponding kinetic equation in the nonuniform external field. Thus far, that was only feasible with the aid of a computer [1,12]. In the “thick”-target approximation, though, the bulk of the multiple scattering comes from areas preceding and successive to the volume reflection. Since therein the particle motion becomes highly overbarrier, and straightens out even relative to the active atomic planes, the rate of a fast particle scattering on atomic nuclei must approach that in an amorphous medium (see analysis at the beginning of Sec. II); hence, the number of nuclear interactions in the whole crystal about equals that in an amorphous target of same material and thickness.

\*bon@kipt.kharkov.ua

*Published by the American Physical Society under the terms of the Creative Commons Attribution 3.0 License. Further distribution of this work must maintain attribution to the author(s) and the published article's title, journal citation, and DOI.*

In the next approximation, however, one must realize that there remains a finite difference between nuclear interaction probability at volume reflection in a bent crystal and in an amorphous target, accumulated in the volume reflection region, whose extent estimates as  $\sim R\theta_c$  [13]. Therefore, for practically used crystals, the mentioned difference must constitute  $\sim 10\%$ , and grow with the increase of the bending radius. Recently, this difference has been measured [14], by subtracting the number of nuclear interactions in the same crystal turned to an “amorphous orientation” (see Sec. II B). It may even have a possible application for diagnostics of the volume reflection dynamics and estimate of its deteriorating effects (with the expectation that the greater the difference, the weaker the deterioration); however, a reliable theory needs to be provided first. Last but not least, the peculiarities of multiple Coulomb scattering in the volume reflection region may be important for the theory of volume capture, which is yet in its infancy.

Setting to evaluate the contribution of nuclear interactions and multiple Coulomb scattering at volume reflection, it appears that for the practically interesting range of beam and crystal parameters, particularly for the conditions of CERN experiments, the multiple Coulomb scattering must be relatively weak and allow for perturbative treatment. Therefore, the number of inelastic nuclear interactions, as well as the mean square angle of multiple Coulomb scattering, must be proportional to the particle range in the regions containing nuclei, and this range may be evaluated along the particle trajectory in the pure continuous potential. Furthermore, for simplification of the calculation, the atomic planes may be treated as infinitesimally thin, whereby the nuclear range in one plane is inversely proportional to the sine of the plane-crossing angle. Then, the problem boils down to evaluation of a sum of inverse plane-crossing angles, and averaging thereof over the impact parameters of particles in the initial beam. In fact, based on the transverse energy conservation law, and even without resorting to model approximations for the interplanar continuous potential (such as those employed in [9]), the entire procedure can be accomplished in closed analytic form, rewarding the simplified approach. The results obtained in this framework were partially published in [15]. In the present paper we will describe their derivation and explore the applicability conditions. We will also discuss the relationship with the volume capture phenomenon.

The plan of our paper is as follows. In Sec. II we carry out the calculation by the principles formulated above, for particles of different charge sign, and different orientations of the silicon crystal: (110) and (111). In Sec. III the limitations of the adopted approach are determined. Section III D gives relevant estimates for the volume capture probability. In Sec. IV A we return to the formulas obtained in Sec. II, applying them to evaluation of the

probability of inelastic nuclear interactions at specific experimental conditions, whereupon the theory is compared with the experiment. In Sec. IV B we extend the theory predictions to the elastic scattering, and address the issue of the volume-reflected beam angular divergence, also bringing the theory into correspondence with the experiment. The summary is given in Sec. V.

## II. PROBABILITY OF NUCLEAR INTERACTION AT VOLUME REFLECTION

### A. Continuous potential and volume reflection

At the beginning, let us recapitulate basic notions of volume reflection, and the parameters of crystals used. The crystal material is usually silicon, and the simplest choice for the family of active planes is (110), which is often employed. In this orientation, the planes are all equidistant with spacing  $d = 1.92 \text{ \AA}$ . Another popular orientation is (111), involving 2 nonequidistant atomic planes within a period. We will be mostly considering case (110), and discuss generalization to (111) later in Sec. II C 2.

Moving at a small angle to a crystallographic plane, the fast charged particle experiences a so-called continuous potential, averaged along the atomic planes, and depending only on the coordinate perpendicular to them. In a silicon crystal, the interplanar continuous potential is nearly parabolic, i.e., harmonic. Besides  $d$ , it is characterized by the well depth  $V_0 = 22.7 \text{ eV}$  [for orientation (110)]. Another useful parameter is the maximal potential gradient  $F$  achieved in the vicinity of the atomic planes; it satisfies the approximate relation

$$Fd \approx 4V_0. \quad (1)$$

The particle motion in the pure continuous potential conserves the so-called transverse energy  $E\dot{r}_\perp^2/2 + V(r_\perp)$ . Depending on whether kinetic transverse energy  $E\dot{r}_\perp^2/2$  is large or not compared to the potential energy, i.e.,  $\dot{r}_\perp$  is large or not compared with  $\theta_c$  defined in the Introduction, the fast particle motion falls into the category of highly overbarrier, or channeled or quasi-channeled [16].

When the crystal is bent to a small angle, i.e., with a bending radius  $R$  greater than all the crystal dimensions, the continuous potential turns to a function of the radius  $r$  relative to the crystal bending axis, and in addition to  $V(r)$ , it involves the centrifugal energy, which due to large distance to the axis (located outside of the crystal) may be linearized in  $r$ . In total, the conserved transverse energy reads

$$E_\perp = \frac{E}{2}\dot{r}^2 + V_{\text{eff}}(r), \quad (2)$$

with

$$V_{\text{eff}}(r) = V(r) - E\frac{r}{R}. \quad (3)$$

The value of  $R$  at which the centrifugal force  $E/R$  equals the maximal gradient  $F$  of the interplanar potential energy is called the critical radius [17,18]:

$$R_c = \frac{E}{F} \approx \frac{Ed}{4V_0} \approx \frac{E}{5 \text{ GeV}} \text{ [cm]}. \quad (4)$$

We will be dealing with values  $R > R_c$ , at which channeling in a bent crystal is sustainable, but be interested in overbarrier particle motion, at which there exists a phenomenon of volume reflection.

The volume reflection assumes the particle entry to a bent crystal with a plane-crossing angle  $\theta_0 \gg \theta_c$ , and inside the crystal, when the plane-crossing angles become  $\sim \theta_c$ , there develops an uncompensated transverse action of the continuous potential on the particle, leading to an aggregate deflection to angle  $\sim \theta_c$ . The extent of the volume reflection region may be assessed by an order of magnitude by approximating the particle trajectory by a straight line; that gives extent  $\sim R\theta_c$ .

Further on, it is useful to estimate the number of planes crossed by the particle within the volume reflection area. At the border of the volume reflection region,

$$E_{\perp} \approx \frac{E}{2} \theta_c^2 \equiv V_0. \quad (5)$$

On the other hand, the energy difference between the neighboring potential barriers equals

$$\Delta V_{\text{eff}}(d) = V_{\text{eff}}(r) - V_{\text{eff}}(r+d) = \frac{Ed}{R}. \quad (6)$$

Thus, the number of atomic planes crossed by the particle on its way to the reflection point is given by the ratio [19]

$$N = \frac{E_{\perp}}{\delta E_{\perp}} \approx \frac{RV_0}{Ed} = \frac{R}{4R_c}. \quad (7)$$

The same number of planes is crossed by the particle after the reflection point.

In fact, when  $N \leq 1$ , the angular distribution of deflected particles is broad, with the width exceeding the mean deflection value; such a pattern is unsuitable for practical purposes. In contrast, when

$$R > 4R_c, \quad (8)$$

i.e.  $N > 1$ , it was shown in [9] that for the case of positively charged particles in a purely harmonic interplanar continuous potential, the outgoing particle angular distribution looks as [see Eq. (72) of [9]] [20]

$$\frac{dw_{\text{cont}}}{d\chi} \approx \frac{N}{\chi_{\text{lim}}} \Theta\left(\frac{\chi_{\text{lim}}}{2N} - |\chi - \langle \chi \rangle|\right), \quad (9)$$

with  $\Theta$  the Heaviside unit step function, and

$$\langle \chi \rangle \approx \chi_{\text{lim}} \left(1 - \frac{1}{2N}\right), \quad \chi_{\text{lim}} = \frac{\pi}{2} \theta_c. \quad (10)$$

The corresponding rms variation of the angles about the mean value evaluates as

$$\sigma_{\text{cont}} = \sqrt{\int d\chi (\chi - \langle \chi \rangle)^2 \frac{dw_{\text{cont}}}{d\chi}} \approx \frac{\chi_{\text{lim}}}{2\sqrt{3}N}. \quad (11)$$

Notably, it decreases with the increase of the crystal bending radius, whereas the mean value (10) tends to a nonzero constant. The fact that with the increase of  $R/R_c$ , the angular distribution of the volume-reflected particles shrinks may be explained by the simultaneous decrease of  $\Delta V_{\text{eff}}(d)$ , whereby the spread of energies at particle crossing of the last potential barrier decreases, and so trajectories of all the particles relative to their reflection points tend to be more similar.

## B. Nuclear interaction events

Turning to nuclear interactions at volume reflection, first of all one notes that since all the atomic nuclei in a perfect crystal are located in planes, we can regard particle crossing of a single atomic plane as an elementary act of nuclear interaction. The surface atomic density of a plane, in the simplest orientation (110), equals  $n_{\text{at}}d$ , where  $n_{\text{at}}$  is the atomic density in the crystal volume. Therefore, the probability of any kind of nuclear interaction in one atomic plane crossed at a tangential angle  $\theta$  is

$$P_1 = n_{\text{at}} \sigma_A \frac{d}{\sin\theta}, \quad (12)$$

$\sigma_A$  being the corresponding cross section on a single nucleus. For elastic scattering one must implement there the transport cross section ( $\sigma_A = \sigma_{\text{tr}}$ ), while for inelastic interactions use the corresponding total inelastic cross section on a silicon nucleus ( $\sigma_A = \sigma_{\text{inel}}$ ) [21].

If we consider a straight crystal, and a highly overbarrier particle, when  $\theta$  by far exceeds the critical value,

$$\theta \gg \theta_c, \quad (13)$$

and thus is subject to negligible variation within the crystal, summing up contributions (12) for  $\approx \frac{L \sin\theta}{d}$  crossed planes yields the total nuclear interaction probability:

$$P = n_{\text{at}} \sigma_A L \begin{pmatrix} \text{straight crystal,} \\ \text{highly overbarrier motion} \end{pmatrix}. \quad (14)$$

This value is independent of  $d$  and  $\theta$ , and is equal to the corresponding probability in an amorphous (i.e. polycrystalline) medium—not surprisingly since the uniform particle flow covers each nucleus with the same density, irrespective of the far atomic order in the medium. In that sense, one can speak about an “amorphous orientation” of a perfect crystal as well. By the same token, the latter notion applies in bent crystal regions where the particle motion is highly overbarrier.

In a bent crystal, however, condition (13) breaks down in a vicinity of the radial reflection point. Since there the plane-crossing angle varies considerably along the particle path, it must be evaluated accurately at each plane

crossing. As mentioned in the Introduction, the simplest way of doing that is to compute the particle trajectory in the pure continuous potential, neglecting the multiple Coulomb scattering. In a uniformly bent crystal (which is a good approximation at the present technology level), the sine of the plane-crossing angle entering Eq. (12) expresses simply as the time derivative of the particle radial coordinate:

$$\sin\theta \approx \dot{r}. \quad (15)$$

Inserting Eq. (15) to Eq. (12) and summing over all the planes crossed by the particle, we obtain the total nuclear interaction probability in a uniformly bent crystal:

$$P \approx n_{\text{at}} \sigma_A d \sum_n \frac{1}{\dot{r}_n}. \quad (16)$$

To isolate the physics associated with volume reflection, we may form a difference between the number of nuclear interactions in an oriented crystal and in an “unoriented” crystal:

$$\Delta P = n_{\text{at}} \sigma_A \Delta L, \quad (17)$$

where factor

$$\Delta L = \sum_n \frac{d}{\dot{r}_n} - L \quad (18)$$

is independent of the detail of nuclear interaction, representing the excess (or deficit) of the target nuclear interaction range. In principle,  $\Delta L$  may depend on both volume and boundary effects,  $\Delta L = \Delta L(R, E, L, \theta_0)$ , but considering that usually the crystal is thicker than the volume reflection region, we will restrict ourselves herein to the thick-crystal limit  $L \rightarrow \infty$ :

$$\Delta L(R, E) = \lim_{L \rightarrow \infty} \left( \sum_n \frac{d}{\dot{r}_n} - L \right). \quad (19)$$

Provided that away from the volume reflection area the particle motion straightens out, the nuclear interaction rate there should approach that in the amorphous medium, so the limit (19) must exist. The rest of this section is dedicated to its evaluation.

Granted the symmetry of the particle trajectory in a centrally symmetric continuous potential with respect to the reflection point, one may count the crossed planes beginning from the reflection point in one direction only (changing the summation index from  $n$  to  $m = n_{\text{max}} - n$ , where  $n_{\text{max}}$  corresponds to the crossed plane nearest to the volume reflection point), and then double the result:

$$\Delta L = 2 \lim_{n_{\text{max}} \rightarrow \infty} \left( \sum_{m=0}^{n_{\text{max}}} \frac{d}{\dot{r}_{n_{\text{max}}-m}} - t_{\text{refl}} \right). \quad (20)$$

Here  $t_{\text{refl}}$  is the distance from the reflection point to the crystal boundary—say, its entry face, where the entrance angle  $\theta_0$  relative to the atomic planes is known (see Fig. 1).

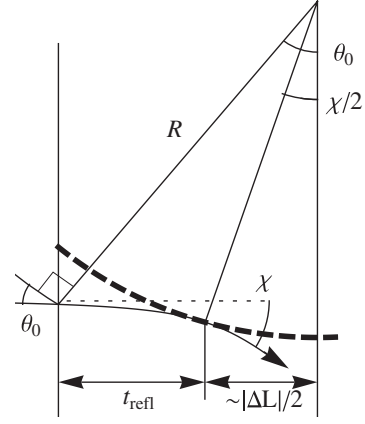


FIG. 1. Relation between the volume reflection angle, the angle of particle entrance to the crystal, the depth of the reflection point, and the crystal bending radius. Dashed arc— one of the bent atomic planes. Solid curve—schematic of the particle trajectory. (The real trajectory remains symmetric with respect to the reflection point, but has some oscillations away from it, though at large distance it straightens out.)

We may express  $t_{\text{refl}}$  in terms of the particle trajectory parameters, too. In fact, at large  $n_{\text{max}}$  it is unambiguously related with the total volume reflection angle  $\chi$ . In the small-angle approximation, from Fig. 1 one infers [22]

$$\chi/2 = \lim_{\theta_0 \rightarrow \infty} (\theta_0 - t_{\text{refl}}/R). \quad (21)$$

Having traded  $t_{\text{refl}}$  for  $\theta_0$ , the latter angle is now to be related with  $n_{\text{max}}$ . But this relation, in fact, appears to be trivial in the thick-crystal limit implying the condition

$$\theta_0 \sim \frac{L}{2R} \gg \theta_c \quad (\text{“thick”-crystal limit}). \quad (22)$$

Acting by the same principle as at evaluation of  $N$  in Sec. II A, but substituting  $\dot{r} = \theta_0$  instead of  $\theta_c$ , and  $V_0/2$  as an average potential energy, we find

$$n_{\text{max}} = \frac{R\theta_0^2}{2d} + \mathcal{O}\left(\frac{V_0 R}{2Ed}\right) \equiv \frac{R\theta_0^2}{2d} + \mathcal{O}\left(\frac{N}{2}\right), \quad (23)$$

where the indeterminacy is related with the dependence of the initial potential energy on the particle impact parameter in the incident beam. Solving Eq. (23) for  $\theta_0$ , we get

$$\theta_0 = \sqrt{\frac{2d}{R}} \left[ \sqrt{n_{\text{max}}} + \mathcal{O}\left(\frac{N}{4\sqrt{n_{\text{max}}}}\right) \right]. \quad (24)$$

Here, the interaction-dependent correction term asymptotically vanishes as  $n_{\text{max}} \rightarrow \infty$ , and may be omitted under the limit sign.

Combining Eqs. (20) and (21) with (23), we cast  $\Delta L$  in the form

$$\Delta L = R\chi[1 + \mathcal{O}(\theta_c R/L)] + 2\sqrt{2Rd} \lim_{n_{\max} \rightarrow \infty} \left( \sum_{m=0}^{n_{\max}} \frac{\sqrt{d/2R}}{\dot{r}_{n_{\max}-m}} - \sqrt{n_{\max}} \right). \quad (25)$$

The inaccuracy  $\mathcal{O}(\theta_c R/L)$  due to the boundary effects appears to be commensurable with the ratio of the volume reflection area and the crystal thickness. Under conditions of CERN SPS experiments, it constitutes  $\sim 1\%$ – $15\%$ , and can be safely neglected.

### C. Summation over atomic planes

#### 1. Orientation (110)

To proceed, we need to evaluate the terms of the sequence of angles  $\dot{r}_n$  entering the denominator in Eq. (25). For a single-well interplanar potential, independently of its precise shape,  $\dot{r}_n$  appears to be a beneficially simple function of the plane order number  $n$ . From Eq. (2) we express

$$\dot{r} = \sqrt{2 \left( \frac{E_{\perp} - V}{E} + \frac{r}{R} \right)}, \quad (26)$$

with  $E_{\perp} = E_{\perp}(\theta_0, b)$  depending on the particle initial conditions including its impact parameter  $b$  and the incidence angle  $\theta_0$  with respect to the planes. Now, granted the periodicity of the intracrystal continuous potential, values of  $V(r)$  are equal at atomic plane locations:

$$V(r_n) = V|_{r \in \text{atomic plane}} = \text{const.} \quad (27)$$

As for  $r$  in the centrifugal energy term in Eq. (26), its value at different atomic planes differs only by a multiple of  $d$ :

$$r_n = r_{n_{\max}} + (n_{\max} - n)d \quad (n \leq n_{\max}). \quad (28)$$

With the account of this, we are able to write

$$\dot{r}_{n_{\max}-m} = \sqrt{2 \frac{d}{R} (\eta + m)}, \quad m = 0, 1, 2, \dots, \quad (29)$$

where variable

$$\eta = \frac{[E_{\perp} - V(r_{n_{\max}})]R}{Ed} + \frac{r_{n_{\max}}}{d} \quad (30)$$

accumulates all the dependence on the initial conditions. In order to secure the relation  $\min\{\dot{r}_n^2\} = \max\{\dot{r}_{n-1}^2\}$ ,  $\eta$  belongs to an interval of unit length:

$$\eta_{\min} < \eta \leq \eta_{\min} + 1. \quad (31)$$

Substituting  $r_{n_{\max}-m}$  from Eq. (29) to Eq. (25), we cast it in the form

$$\Delta L = R\chi + \sqrt{2Rd} \zeta\left(\frac{1}{2}, \eta\right) \quad [\text{Si}(110)], \quad (32)$$

where

$$\zeta\left(\frac{1}{2}, \eta\right) = \lim_{n_{\max} \rightarrow \infty} \left( \sum_{m=0}^{n_{\max}} \frac{1}{\sqrt{\eta + m}} - 2\sqrt{n_{\max}} \right). \quad (33)$$

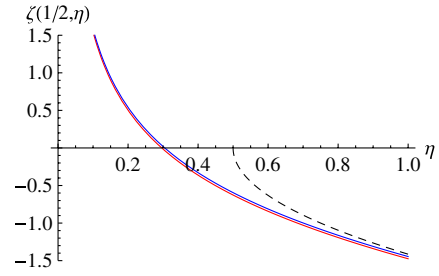


FIG. 2. Blue curve—behavior of Hurwitz zeta function  $\zeta\left(\frac{1}{2}, \eta\right)$  given by Eq. (33); red curve—its approximation (34); black dashed curve—approximation (35) becoming neat for  $\eta > 1$ . The integral from function  $\zeta\left(\frac{1}{2}, \eta\right)$  over the displayed interval  $0 < \eta \leq 1$  equals zero [Eq. (43)].

The latter limit is categorized as Hurwitz (or generalized Riemann) zeta function with the parameter equal  $\frac{1}{2}$  [for a general definition of  $\zeta(\alpha, \nu)$  see [23]]. For all practical purposes, it may be approximated by

$$\zeta\left(\frac{1}{2}, \eta\right) \approx \frac{1}{\sqrt{\eta}} + \frac{1}{2\sqrt{\eta+1}} - 2\sqrt{\eta+1}, \quad \forall \eta, \quad (34)$$

obtained by application to the sum in (33) (after isolation of the first, singular term) of the Euler-Maclaurin formula [24]. Furthermore, at  $\eta > 1$  it admits a simpler approximation:

$$\zeta\left(\frac{1}{2}, \eta\right) \approx -2\sqrt{\eta - \frac{1}{2}} \quad (\eta > 1) \quad (35)$$

(see Fig. 2).

#### 2. Orientation (111)

In the case of orientation (111), the continuous potential values at all the planes are still equal, but the interplanar intervals assume alternating values  $d/4$  and  $3d/4$ . The principle of calculation remains the same, except that the summation over the atomic planes is to be performed separately for odd and even numbers. The result then involves two different  $\zeta$  functions:

$$\Delta L = R\chi + \sqrt{\frac{Rd}{2}} \left[ \zeta\left(\frac{1}{2}, \eta_1\right) + \zeta\left(\frac{1}{2}, \eta_2\right) \right] \quad [\text{Si}(111)], \quad (36)$$

where depending on which of the nonequivalent planes is encountered the last,

$$\eta_{\min} < \eta_1 \leq \eta_{\min} + \frac{3}{4}, \quad \eta_2 = \eta_1 + \frac{1}{4} \quad (37a)$$

or

$$\eta_{\min} < \eta_1 \leq \eta_{\min} + \frac{1}{4}, \quad \eta_2 = \eta_1 + \frac{3}{4} \quad (37b)$$

For positive particles, the probability of case (37a) equals  $3/4$ , while that of case (37b) equals  $1/4$ . For negative particles at  $R > 4R_c$  the case (37a) is realized with the

unit probability, inasmuch as the higher potential barriers completely shadow the adjacent minor ones, despite the centrifugal energy tilt.

So far the analysis applied for particles of any charge sign. But in what concerns the last unknown quantity  $\eta_{\min}$ , the situation turns principally different for positively and for negatively charged particles. Below we shall scrutinize these two cases separately.

## D. Determination of $\eta_{\min}$ and averaging over the particle initial conditions

### 1. Positively charged particles

In the case of positively charged particles (typically protons), determination of  $\eta_{\min}$  is the simplest. Consider, again, the case of orientation (110). At particle entrance to the reflection interval [see Fig. 3(a)], the minimum of the kinetic energy is achieved when the particle passes the last potential barrier with a vanishing kinetic energy on its top. But for positively charged particles, that barrier coincides with the atomic plane, the kinetic energy on which we desire to know. So, at  $\eta_{\min}$  this energy merely turns to zero:

$$\min\{\dot{r}_{n_{\max}}^2\} = 0 \Rightarrow \eta_{\min} = \frac{R}{2d} \min\{\dot{r}_{n_{\max}}^2\} = 0. \quad (38)$$

Thus,  $\eta$  belongs to the interval  $0 < \eta \leq 1$  (actually exhibited in Fig. 2). The divergence of function  $\zeta(1/2, \eta)$  at the physical interval end point  $\eta \rightarrow 0$  corresponds to a grazing crossing of the last atomic plane. The other end point value equals  $\zeta(1/2, 1) = \zeta(1/2) \approx -1.46$ . Note that with the known lower limit (38),  $\eta$  may be found even without the need to evaluate  $n_{\max}$ , if one rewrites Eq. (30) as

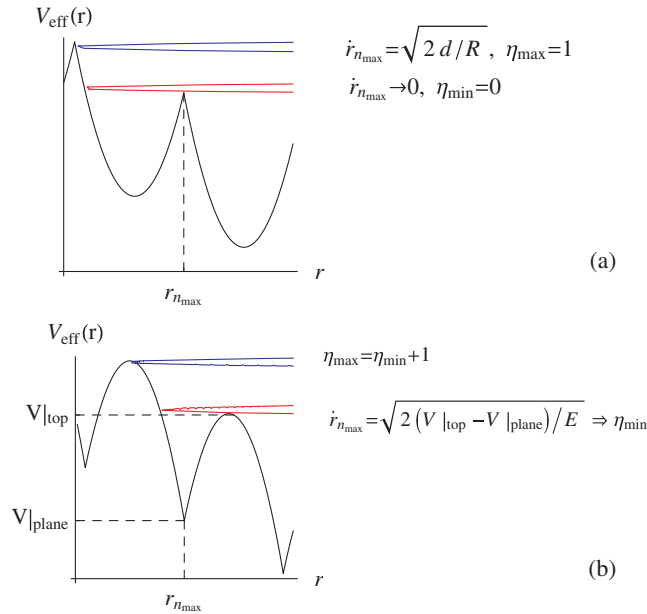


FIG. 3. Determination of the range of variation of parameter  $\eta$  in crystal orientation (110); (a) for positively charged particles; (b) for negatively charged particles. For details see text.

$$\eta \equiv \{\eta\}_f = \left\{ \frac{(E_{\perp} - V)|_{r \in \text{at. plane}} R}{Ed} + \frac{r_{\text{plane}}}{d} \right\}_f, \quad (39)$$

with braces  $\{\}_f$  signifying the operation of taking the fractional part, and  $r_{\text{plane}}$  representing  $r$  at any atomic plane (with the same result after the  $\{\}_f$  operation).

Since at  $\eta \lesssim 1$  typical values of function  $\zeta$  are  $\sim 1$ , the ratio of the two terms in (32) is of the order

$$\frac{\sqrt{2Rd}}{R\theta_c} = \sqrt{\frac{R_c F_{\max} d}{RV_0}} \approx \frac{1}{\sqrt{N}} < 1. \quad (40)$$

But in actual practice, that ratio may still be sizable, especially at  $\eta \rightarrow 0$  where the  $\zeta$  function blows up. Then, it might seem that  $\eta$  must necessarily be specified issuing from the initial conditions.

However, one should remember that in a real beam the initial conditions for the particle entrance to the crystal are not strictly definite. The beam transverse dimensions are always much greater than interatomic distances in the crystal, therefore the particle impact parameters  $b$  must be averaged over. Besides that, the indeterminacy  $\delta\theta_0$  of the angles in the incident beam is usually large compared to  $d/L$ , and needs some averaging in a vicinity of the mean value  $\theta_0$ .

Examining Eq. (39), we see that the expression under the fractional part sign contains contributions from the initial kinetic and potential energies in an additive way:  $E_{\perp} = \frac{E}{2}\theta_0^2 + V(b)$ . Actually, fluctuations of both contributions are large:

$$\delta\left(\frac{R}{Ed} \frac{E}{2} \theta_0^2\right) \approx \frac{R\theta_0}{d} \delta\theta_0 \sim \frac{L}{2d} \delta\theta_0 \gg 1, \quad (41)$$

and

$$\delta\left(\frac{R}{Ed} V\right) \sim N > 1. \quad (42)$$

Thus, at fluctuations of particle parameters in a real beam,  $\eta$  spans its unit definition interval many times, and at each time its relation with  $\theta_0$  and  $b$  is approximately linear, so, in fact,  $\eta$  may be treated as a uniformly distributed random variable. Then, averaging over the beam is equivalent to an unweighted averaging over  $\eta$ . But such an average of function  $\zeta$  entering (32) gives zero due to identity

$$\int_0^1 d\eta \zeta\left(\frac{1}{2}, \eta\right) = 0, \quad (43)$$

straightforwardly checkable from definition (33). That ultimately leads to a simple and model-independent relation of the mean excess of the nuclear range at volume reflection with the mean volume reflection angle:

$$\langle \Delta L \rangle = R \langle \chi \rangle \quad (\text{positively charged particles}). \quad (44)$$

The accuracy of Eq. (44) is an interesting question. Within the adopted approximation of thin atomic planes linked by a pure continuous potential, the only parameter

in the problem is  $N$ , which is further assumed to be large. We found fortuitous vanishing of the term of relative significance  $\mathcal{O}(N^{-1/2})$ , but this does not mean that we deal with an expansion in powers of  $N^{-1/2}$ . The inaccuracy of Eq. (44) stems from replacing the averaging over  $b$  by averaging over  $\eta$  (or  $E_{\perp}$ ). This approximation must work better than  $\mathcal{O}(N^{-1})$ , presumably as  $\mathcal{O}(N^{-2})$  (cf. [9]). However, one should not forget about physical corrections due the approximation of thin planes and the pure continuous potential in itself, which can be actually more significant. The corresponding estimates will be provided in Sec. III.

For the case of orientation (111), the calculation is a bit more involved, but straightforward. Interestingly, one arrives at the same result (44).

## 2. Negatively charged particles

For negatively charged particles (such as  $\pi^{-}$ ), the situation is different in that the atomic plane positions do not coincide with tops of the potential barriers – thus, here  $\eta_{\min} \neq 0$  [see Fig. 3(b)]. To determine the value of  $\eta_{\min}$ , we need to know the particle kinetic energy at the last plane crossing, which in the present case equals the difference of potential energies between the atomic plane and the top of the preceding barrier:

$$\frac{E}{2} \min r_{n_{\max}}^2 = V|_{r \in \text{top}} - V|_{r \in \text{plane}} \approx V_0 \left(1 - \frac{R_c}{R}\right)^2. \quad (45)$$

Here, the last equality would be exact for a parabolic interplanar potential, while for a nonparabolic one it also turns to be exact in the limits  $R \gg R_c$  and  $R \rightarrow R_c$ . So, heuristically, we may expect it to be sufficiently accurate over the entire interval  $R > R_c$ . Therewith, we get

$$\eta_{\min} = \frac{R}{2d} \min r_{n_{\max}}^2 \approx N \left(1 - \frac{1}{4N}\right)^2. \quad (46)$$

Here the prefactor must be  $> 1$  [see Eq. (8)]. From Fig. 2 we see that at  $\eta > 1$ , function  $\zeta(1/2, \eta)$  is fairly smooth and may be linearized in  $\eta$  about the midpoint  $\eta_{\min} + 1/2$ . Taylor expanding Eq. (35), we obtain

$$\zeta\left(\frac{1}{2}, \eta\right) \approx -2\sqrt{\eta_{\min}} - \frac{1}{\sqrt{\eta_{\min}}} \left(\eta - \eta_{\min} - \frac{1}{2}\right). \quad (47)$$

Averaging the last term of Eq. (47) over the interval  $\eta \in (\eta_{\min}, \eta_{\min} + 1]$  gives zero. Substituting in the first term of (47)  $\eta_{\min}$  from Eq. (46), and all that to Eq. (32), we obtain the final expression for the average nuclear range difference in the case of (110) orientation:

$$\langle \Delta L \rangle = R \langle \chi \rangle - 2R\theta_c \left(1 - \frac{R_c}{R}\right) \quad (48)$$

[negatively charged particles, Si(110)].

At  $R \gg 4R_c$ , when  $\langle \chi \rangle \approx \theta_c$ , Eq. (48) reduces to

$$\langle \Delta L \rangle \approx -R\theta_c. \quad (49)$$

For orientation (111) in the negative particle case the calculation is more complicated. We will quote the result under the condition  $R > 4R_c$ , retaining only the linear correction in  $R_c/R$ , which is relatively simple:

$$\langle \Delta L \rangle = R \langle \chi \rangle - 2R\theta_c \left(1 - \frac{5R_c}{3R}\right) \quad (50)$$

[negatively charged particles, Si(111)].

Here we define  $\theta_c = \sqrt{2V_L/E}$ , and  $R_c \approx \frac{3Ed}{16V_L}$ , with  $V_L$  the larger well depth in a straight crystal (see [18]).

Equations (44) and (49) were reported in [15]. We stress that for positive particles the nuclear range excess is positive, while for negative particles it is negative (representing a deficit), though being of the same order of magnitude. This is natural from the point of view that positive particles are repelled from the atomic planes, crossing them more tangentially, while negative particles are attracted, crossing the planes more quickly. For multiple Coulomb scattering, such an effect was noticed in numerical simulation already in the pioneering paper [1].

On the practical side, for measurement of the nuclear interaction excess compared to the amorphous orientation, it may appear easier to actually deal with the difference between volume reflection of positively and negatively charged particles in the same bent crystal, inasmuch as the latter difference is about doubled.

## III. CONDITIONS OF APPLICABILITY

The simplified account of nuclear interactions in the previous section rested on a few assumptions. Prior to proceeding to comparison with the experiment, let us determine their conditions of validity, in terms of the crystal and the beam parameters. For simplicity, we restrict ourselves to the positive particle case, which has received more experimental attention.

### A. Spread of nuclear concentrations in atomic planes

The first approximation we made in Eq. (16) is the neglect of fluctuations of nuclei about the atomic planes. In fact, even at zero temperature, there remains quantum indeterminacy of the same order of magnitude as the thermal fluctuations at room temperature. For a crude estimate of a nucleus departure from its equilibrium position, in projection onto direction perpendicular to the active plane, a harmonic oscillator model may be adopted. For an oscillator with typical frequency  $\omega_0$ , the mean square coordinate of the nucleus at a temperature  $\mathcal{T}$  equals

$$\langle (\delta X)^2 \rangle = \frac{\hbar}{2M\omega_0} \coth \frac{\hbar\omega_0}{2k\mathcal{T}}, \quad (51)$$

where  $M$  is the nucleus mass, and  $k$  the Boltzmann constant. In a solid state, a satisfactory estimate for  $\omega_0$  is

$$\hbar \omega_0 \approx \sqrt{3kT_D}, \quad (52)$$

where  $T_D$  is the Debye temperature [25]. For silicon,  $T_D \approx 650$  K. Based on these crude estimates, we retrieve the value  $u \sim 0.05$  Å for the spread of nuclei about any plane in a silicon crystal at room temperature (see also [26]).

Our approximation of thin nuclear concentrations will be valid if relative variation of  $r$  within  $u$  is small. That is to say, the variation of the kinetic energy  $E \frac{r^2}{2}$  must be relatively small. But the total transverse energy (2) is conserved, thus the variation of the kinetic energy equals to the (minus) variation of the effective potential energy. At the distance of nuclear fluctuations, the variation of the potential energy equals the height of the nuclear cap on the top of the potential barrier (the centrifugal energy may be neglected):

$$\delta V|_{\text{nucl}} = \frac{Fu}{2} \approx 1.5 \text{ eV}. \quad (53)$$

This quantity is to be compared with the kinetic energy of a particle at the last atomic plane crossing, which for positively charged particles has the order of the (half) potential energy difference (6) between the neighboring barriers:

$$E_{\text{kin}}|_{n_{\text{max}}} \sim \frac{1}{2} \Delta V_{\text{eff}}(d). \quad (54)$$

From condition  $\delta V|_{\text{nucl}} \ll E_{\text{kin}}|_{n_{\text{max}}}$ , one derives a restriction on the crystal bending radius as a function of the particle energy and crystal temperature:

$$R \ll R_u(E, T) \quad (\text{thin nuclear concentration}), \quad (55)$$

where

$$R_u(E, T) = \frac{Ed}{Fu} = \frac{R_c d}{u} \quad (\text{positively charged particles}). \quad (56)$$

Obviously, it holds that  $R_u \gg 4R_c$  until the crystal temperature rises so that  $u \sim d/4$ , whereat the crystal may already melt. At room temperature,  $\frac{R_u}{4R_c} \sim \frac{d}{4u} \approx 10$ , so the double inequality  $4R_c < R \ll R_u$  may be well satisfied.

## B. Dominance of the continuous potential

In order that multiple Coulomb scattering in the crystal bulk did not overwhelm the volume reflection effect, at practice the crystal thickness is always made sufficiently small, such that the rms angle of multiple scattering is small compared to  $\chi \sim \theta_c$ :

$$\sigma_{\text{am}} \ll \theta_c. \quad (57)$$

However, that condition does not yet guarantee that multiple scattering has little effect on  $\Delta L$ , because in the volume reflection region the angles of plane crossing are  $\ll \theta_c$ , as well. Taking as the smallest and the most

vulnerable dynamical angle that of the last atomic plane crossing,  $\dot{r}_{n_{\text{max}}}$ , the average  $\dot{r}_{n_{\text{max}}}$  for positively charged particles, may be estimated from Eq. (29) as

$$\langle \dot{r}_{n_{\text{max}}} \rangle = \int_0^1 d\eta \dot{r}_{n_{\text{max}}} = \frac{2}{3} \sqrt{\frac{2d}{R}} \approx \sqrt{\frac{d}{R}}. \quad (58)$$

[The corresponding transverse kinetic energy  $\frac{E}{2} \langle \dot{r}_{n_{\text{max}}} \rangle^2 \approx \frac{1}{2} \Delta V_{\text{eff}}(d)$  equals half the potential energy difference between neighboring barriers.] In contrast to  $\theta_c$ ,  $\langle \dot{r}_{n_{\text{max}}} \rangle$  does not depend on the particle energy, instead involving the crystal bending radius, but at particle energies and crystal radii suitable for volume reflection,

$$\frac{\langle \dot{r}_{n_{\text{max}}} \rangle}{\theta_c} \sim \frac{1}{\sqrt{2N}} < 1. \quad (59)$$

The effective rms angle of multiple Coulomb scattering (in projection onto *one* relevant transverse direction perpendicular to the active family of atomic planes) is determined by the Highland-Lynch-Dahl Gaussian fit [27,28]:

$$\sigma_{\text{am}}(T) = \frac{13.6 \text{ MeV}}{E} \sqrt{\frac{T}{X_0}} \left( 1 + 0.038 \ln \frac{T}{X_0} \right) \quad (60)$$

$$(10^{-3} < T/X_0 < 10^2), \quad (61)$$

with  $T$  the traversed material thickness, and  $X_0$  the material-dependent radiation length (for silicon this constant equals  $X_0 \approx 9.36$  cm). The logarithm of  $T$  in Eq. (60) owes to the Rutherford large-angle ‘‘tail’’ of multiple scattering, violating under conditions (61) the Gaussianity of the profile in principle, though weakly. Formula (60) works with an accuracy of a few percent for high- and intermediate- $Z$  media. Around  $T \sim 0.2 \div 1$  mm, i.e., with  $1 + 0.038 \ln \frac{T}{X_0} \approx 0.8 \pm 0.03$ , Eq. (60) may be used in a simplified form:

$$\sigma_{\text{am}}(T) \approx \frac{11 \text{ MeV}}{E} \sqrt{\frac{T}{X_0}}, \quad (62)$$

obeying the property of square additivity  $\sigma_{\text{am}}^2(T_1 + T_2) = \sigma_{\text{am}}^2(T_1) + \sigma_{\text{am}}^2(T_2)$ . The obtained coefficient 11 MeV in (62) is smaller than estimate  $\sqrt{\frac{4\pi}{\alpha}} \frac{m}{\sqrt{2}} = \frac{21.2 \text{ MeV}}{\sqrt{2}} \approx 14.8$  MeV often used within the simplest leading logarithmic approximation [29].

Inserting  $T \sim R\theta_c$  into Eq. (62), and dividing by Eq. (58), we arrive at a requirement,

$$\frac{\sigma_{\text{am}}(R\theta_c)}{\langle \dot{r}_{n_{\text{max}}} \rangle} \approx R \frac{11 \text{ MeV}}{E} \sqrt{\frac{\theta_c}{X_0 d}} \ll 1, \quad (63a)$$

which may be viewed as a restriction on the crystal bending radius,

$$R \ll R_{\text{mult}}(E) \quad (\text{continuous potential dominance}), \quad (63b)$$

if we introduce

$$R_{\text{mult}}(E) = \frac{E}{11 \text{ MeV}} \sqrt{\frac{X_0 d}{\theta_c}} = \left( \frac{E}{18 \text{ GeV}} \right)^{5/4} [\text{m}] \quad (64)$$

(positively charged particles).

From Eqs. (4) and (64) we notice that at relativistic particle energies, definitely,  $R_{\text{mult}} \gg 4R_c$ , so there is enough room for double inequality  $4R_c < R \ll R_{\text{mult}}$  to hold.

Condition (63b), in principle, may be significant not only for equations describing the excess of nuclear interaction probability, but for the volume reflection robustness as a whole. The impact of multiple scattering may result in more uniform distribution of the particle flow over the crystal volume, whereat contributions from positive and negative force regions will become less unequal. In particular, that may lead to a suppression of the mean angle of volume reflection at  $R > R_{\text{mult}}$ , which, however, is difficult to estimate in the context of the perturbative approach.

### C. Combined conditions

Simultaneous fulfilment of conditions (8), (56), and (64) guarantees our calculation of the nuclear interaction probability at volume reflection to be self-consistent. In Fig. 4 we assemble all those conditions as functions of the particle energy. As we observe, they allow for a sufficiently broad corridor (green band in Fig. 4), extending to arbitrarily high energies.

Conditions (56) and (64) appear to be rather close (at list for silicon), and at  $E \sim 40 \text{ GeV}$ ,  $R \sim 2 \text{ m}$  they have an intersection point. Sector  $R_u < R < R_{\text{mult}}$  (yellow wedge in Fig. 4) is acceptable for realization of volume reflection, but not for our formulas for the nuclear interaction excess.

Points in Fig. 4 indicate parameters of the world experiments on volume reflection. [Some of them are actually for

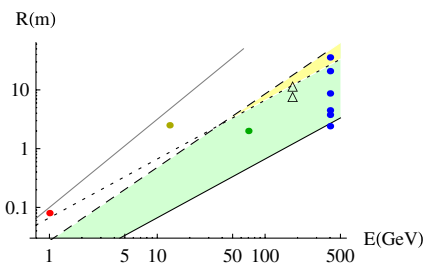


FIG. 4. Combined plot of conditions for volume reflection of charged particles in a silicon crystal, and the parameters of the related experiments. Solid black line—condition (8); dashed line—Eq. (64); dotted—Eq. (56); solid gray line—volume capture (73). Blue points—experiments at CERN SPS, 400 GeV protons, orientation (110) [32]; green—IPEP at 70 GeV, orientation (111) [2]; yellow—CERN PS at 13 GeV, orientation (110) [5]; red—PNPI at 1 GeV, orientation (111) [3]. Triangles—experiment at CERN SPS, 180 GeV electrons and positrons, crystal orientation (111) [33]. The colored band indicates the region best suited for volume reflection. For discussion see text.

(111) crystal orientation, but may serve for qualitative demonstration.] As we see, CERN SPS experiment spans exactly the band best suited for volume reflection, whereas experiments at 1 and 15 GeV probe other interesting regions.

### D. Volume capture and volume reflection inefficiency

Although conditions (8), (56), and (64) seem to basically suffice for the validity of the derived Eqs. (17), (44), and (49), there may arise an extra question concerning the effect of capturing of some of the volume-reflecting particles to channeling states (volume capture) and their subsequent dechanneling. If the capture happens near the top of the potential barrier, the particle oscillation amplitude in the channel is large, so it dechannels within a short distance, and may emerge at angles adjacent to the volume reflection peak. Phenomenologically, there is indeed observed a thrust in the otherwise Gaussian volume reflection peak extending to the crystal bending direction. The fraction of particles belonging to this thrust is called the volume reflection inefficiency. For completeness, in this subsection we will provide some conservative estimates for the probability of the volume capture process.

First of all, it is instructive to estimate how local are the collisions between two relativistic particles with a sizable transverse energy exchange  $\delta E_{\perp} \sim E_{\perp} \sim \frac{Fu}{2}$ . The transferred momentum

$$\delta q \sim \sqrt{2EE_{\perp}} \quad (65)$$

corresponds to a typical impact parameter

$$b \sim \min \left\{ \frac{\hbar}{\delta q}, \frac{Ze^2}{\delta q} \right\} = \frac{\hbar}{\delta q} \sim \frac{\hbar}{\sqrt{EFu}} \sim u \left( \frac{0.04 \text{ \AA}}{u} \right)^{3/2} \sqrt{\frac{\text{GeV}}{E}}. \quad (66)$$

At  $u \geq 0.05 \text{ \AA}$ , and  $E \gg 1 \text{ GeV}$ , Eq. (66) implies  $b \ll u$ , so the scattering process leading to volume capture may be regarded as sufficiently local. If the scattering is multiple, at sufficiently high energy it also remains local, and may be described as a diffusion in the particle transverse velocities, with the diffusion coefficient proportional to the local nuclear density. Within the area of nuclear concentration in an atomic plane, the nuclear density is of the order

$$\rho = \frac{d}{2u} \rho_0, \quad (67)$$

where  $\rho_0$  is the net density of atoms in the crystal. The incoherent scattering on atomic electrons may be neglected in the first approximation.

Now consider a particle having arbitrary transverse kinetic energy  $\tilde{E}_{\perp}$  on the top of a potential barrier; its past history (which may as well include some amount of multiple scattering) is irrelevant. Let us estimate conditions at which this particle will be likely to lose a substantial fraction of its transverse kinetic energy after having rolled

down the hill to distance  $u$ —then, its total transverse energy may become underbarrier. Assuming that the particle motion is still governed predominantly by the continuous potential, the time spent by the particle in the region populated by atomic nuclei equals

$$T_1 = \int_0^u \frac{dr}{\dot{r}} = \int_0^u \frac{dr}{\sqrt{\frac{F}{Eu} r^2 + \frac{2\tilde{E}_\perp}{E}}} = \sqrt{\frac{Eu}{F}} \operatorname{arsinh} \sqrt{\frac{Fu}{2\tilde{E}_\perp}}. \quad (68)$$

Traversing distance  $T_1$  in nuclear density (67), the particle will acquire angular spread

$$\delta\dot{r} = \frac{11 \text{ MeV}}{E} \sqrt{\frac{T_1}{X_0} \frac{d}{2u}} = \frac{11 \text{ MeV}}{E^{3/4} (Fu)^{1/4}} \sqrt{\frac{d}{2X_0} \operatorname{arsinh} \sqrt{\frac{Fu}{2\tilde{E}_\perp}}}. \quad (69)$$

This can compete with the initial transverse velocity on top of the potential barrier

$$\dot{r}|_{\text{top}} = \sqrt{2\tilde{E}_\perp/E} \quad (70)$$

provided

$$\begin{aligned} \tilde{E}_\perp &= \frac{E}{2} (\dot{r}|_{\text{top}})^2 \\ &= \frac{(11 \text{ MeV})^2}{4\sqrt{EFu}} \frac{d}{X_0} \operatorname{arsinh} \sqrt{\frac{Fu}{2\tilde{E}_\perp}} \sim 1 \text{ eV} \sqrt{\frac{\text{GeV}}{E}}. \end{aligned} \quad (71)$$

The first consequence of this result is that at  $E \gg 1 \text{ GeV}$ , apparently,  $\tilde{E}_\perp \ll Fu$  [that enabled us to replace in (71)  $\operatorname{arsinh} \sqrt{Fu/2\tilde{E}_\perp} \sim \ln \sqrt{2Fu/\tilde{E}_\perp} \sim 2$ ]. Under condition (56), this will also imply  $\tilde{E}_\perp \ll \Delta V_{\text{eff}}(d)$ , whereby the volume capture can occur only at the last plane crossing, and its probability equals

$$P_{\text{capt}}(R, E) \leq \frac{\tilde{E}_\perp}{\Delta V_{\text{eff}}(d)} = 10 \frac{R}{\text{m}} \left( \frac{\text{GeV}}{E} \right)^{3/2}. \quad (72)$$

Numerically, this gives  $P_{\text{capt}}(10 \text{ m}, 400 \text{ GeV}) \sim 4\%$ ,  $P_{\text{capt}}(0.72 \text{ m}, 70 \text{ GeV}) \sim 20\%$ , which does not contradict to experiments and numerical simulation.

Result (72) may be converted into a characteristic radius of volume capture

$$R_{\text{capt}}(E) = \frac{1}{10} \left( \frac{E}{\text{GeV}} \right)^{3/2} [\text{m}], \quad (73)$$

obtained by letting in (72)  $P_{\text{capt}} \sim 1$ . In Fig. 4 it is shown by a gray line. This line goes above  $R_u(E)$ ,  $R_{\text{mult}}(E)$  practically at all energies, so under conditions best suited for volume reflection (the colored band in Fig. 4), volume capture plays a minor role, while for experiments [2,3] it may be significant.

As for the obtained estimate (72) itself, it is interesting to note that it obeys the scaling law  $P_{\text{capt}} \propto RE^{-3/2}$  proposed

in [30]. However, our analysis suggests a different pattern of the particle capture: the smallness of  $\tilde{E}_\perp$  permits capture at one barrier only, whereas Refs. [12,30] assume capture events to happen over the entire volume reflection area  $\sim R\theta_c$  [containing many planes, according to Eq. (7)], and presume statistical equilibrium of volume-reflecting and channeled particle fractions over this region (which for one particle should mean that it passes from overbarrier to underbarrier states and back many times).

Besides the difference in the physical approach, our result differs from [30] by the coefficient at the power law  $RE^{-3/2}$ , most notably by the factor  $Z\sqrt{\frac{d}{2u}}$ . Interestingly, it indicates that  $P_{\text{capt}}$  must decrease with the increase of  $u$ , i.e., with the increase of the crystal temperature, in contrast to the dechanneling probability. In [31], there was proposed a correction factor to [30], which, however, scales as  $u^{-1}$ , rather than  $u^{-1/2}$ .

Admittedly, the pattern of particle capture at one last plane may need modification when  $R > R_u$ , because thereat the particles hitting the back wall of the well may descend to underbarrier energies, too. On the other hand, thereat the dechanneling doubles, and it is unobvious whether the captured particle fraction will increase or decrease. Experimentally, it is established that at larger  $R$ , the increase of the volume reflection inefficiency with  $R$  slows down [32].

At yet greater  $R$ , when  $R \geq R_{\text{capt}}(E)$ , the capture acts can really occur at various planes along the volume reflection area  $\sim R\theta_c$ , and the situation may in some sense approach the statistical equilibrium, with the crystal bend being just adiabatic.

In conclusion, let us remark that in principle, volume capture may be not the only source of volume reflection inefficiency. In a pure continuous potential of a bent crystal, there exists an effect of orbiting (see [9] and references therein), arising due to a retention of the particles on the round top of a potential barrier, which turns as the crystal bends, and it leads to an exponential tail in the angular distribution of the volume-reflected particles, towards the side of the crystal bending. This manifested itself already in Eq. (68) where the  $\operatorname{arsinh}$  diverges as  $\tilde{E}_\perp \rightarrow 0$ . Orbiting is stronger for negative particles, because for them the potential energy around the barrier top is flatter, but for positive particles, with the account of smearing of the atomic planes, orbiting is possible, too. With the increase of  $R/R_c$ , the fraction of orbiting particles increases, but, as was mentioned in Sec. II A, the angular distribution shrinks as a whole.

However, if one takes into account the multiple scattering, its effect is to hinder the particles, too. Furthermore, as we saw in Eqs. (68) and (69), the extension of the nuclear range due to orbiting enhances the multiple scattering, which in turn may detain the particles on top of a curved potential ridge, extending the tail of the angular distribution of exiting particles in the direction of the crystal

bending. We may hypothesize that cooperating in this way, orbiting and multiple scattering may contribute to the inefficiency of volume reflection beyond the volume capture mechanism, but that needs more quantitative investigation than we can provide herein.

## IV. COMPARISON WITH EXPERIMENTS

### A. Inelastic nuclear interaction probability

Now we are in a position to test the predictions of Sec. II against the available experimental data. The most direct check is supposed to be against the results of experiments on inelastic nuclear scattering. At present, there is one such experiment, performed with 400 GeV protons and a  $L = 2$  mm thick silicon crystal at a single value of the crystal bending radius  $R = 10$  m [14].

In this experiment volume reflection conditions were investigated along with those of channeling, and therefore the number of inelastic nuclear interaction events was actually measured vs the varying cutting angle  $\delta\theta_0$  (essentially the initial beam collimation angle). When the cutting angle was sufficiently large (which ought to correspond to perfect averaging over  $b$  or  $E_\perp$ ), the measured relative difference was about constant, holding on the level

$$\frac{\Delta P}{P} \approx (5 \pm 2)\%. \quad (74)$$

For comparison, our prediction, using the experimentally determined mean value  $\langle\chi\rangle_{\text{exp}} = 13.35 \mu\text{rad}$  at the given bending radius  $R = 10$  m, amounts to

$$\frac{\Delta P}{P} = \frac{\langle\Delta L\rangle}{L} = \frac{R\langle\chi\rangle_{\text{exp}}}{L} = 6.67\%. \quad (75)$$

The theoretical accuracy of prediction (75) can be estimated as  $\mathcal{O}(R/R_u)$  [see Eq. (56)]. With  $R = 10$  m and

$$R_u(400 \text{ GeV}) \approx 27 \text{ m},$$

we infer  $R/R_u \approx 1/3$ . That estimate of the accuracy is commensurable with the relative difference between our theory and the experiment [Eqs. (74) and (75)].

A curious feature found in Fig. 6 of [14] is that at small cutting angles ( $\lesssim 2 \mu\text{rad}$ ), the difference between the rate of inelastic nuclear interactions at volume reflection and in an amorphous case seems to depart from a constant and actually vanish, although experimental errors in this region are too high for an unambiguous conclusion. In principle, some sensitivity to  $\delta\theta_0$  might emerge due to an imperfect averaging over the particle initial conditions and to the impact of the second term in Eq. (32). To check this possibility, let us estimate the range of variation of the argument  $\eta$  under the variation of  $\theta_0$  in an interval  $\delta\theta_0 \sim 2 \mu\text{rad}$ . From Eq. (41) we get

$$\delta\eta = \frac{R}{d}\theta_0\delta\theta_0 \sim \frac{L}{2d}\delta\theta_0 \sim 10. \quad (76)$$

Apparently, this number is still much greater than the unit definition interval of variable  $\eta$ ; hence, with the variation of  $\theta_0$  in that range,  $\eta$  actually scans its definition interval several times, i.e., cutting angles down to  $\sim 1 \mu\text{rad}$  still can have no significant impact on  $\Delta L$ . So, we can only attribute the small-cutting-angle fluctuation of  $\langle\Delta L\rangle$  to enhanced experimental errors reflecting the difficulty of achieving such small cutting angles.

### B. Angular divergence of the volume-reflected beam

Measurement of inelastic nuclear scattering discussed in the previous section demands the usage of some dedicated instrumentation like the beam loss monitors. But even without it, the nuclear interactions shall manifest themselves through an angular broadening of the final beam due to elastic Coulomb scattering. A complication here arises because of an additional contribution to the broadening from the impact parameter dependence of the deflection angle, even in a pure continuous potential [see Eq. (4)]. In fact, the latter contribution is anisotropic, but the beam spread transverse to the direction of deflection is rarely measured, so in the published experimental data on the beam dispersion in the direction of deflection they contribute together. Again, the bulk of the broadening is accumulated away from the volume reflection region, but we suppose the latter contribution to be subtractable. The theoretical problem, then, is to compute the difference of the volume reflection case from the amorphous orientation, and the difference between the positive and negative particle cases.

To prove the possibility of the unambiguous subtraction, even though in the whole crystal the multiple scattering is stronger than in the intrinsic volume reflection region alone, let us decompose the kinetics of the particle passage through the crystal into three distinct stages: pure incoherent multiple scattering upstream the volume reflection region (where the beam acquires Gaussian shape), pure dynamical broadening in the volume reflection region, and pure incoherent multiple scattering downstream of it. The resulting angular distribution function expresses as a convolution of probability distributions of the subsequent processes:

$$\begin{aligned} \frac{dw}{d\chi} &= \int d\chi_2 \frac{e^{-[(\chi-\chi_2)^2/2\sigma_2^2]}}{\sqrt{2\pi}\sigma_2} \int d\chi_1 \frac{dw_{\text{cont}}(\chi_2 - \chi_1)}{d(\chi_2 - \chi_1)} \\ &\quad \times \frac{e^{-(\chi_1^2/2\sigma_1^2)}}{\sqrt{2\pi}\sigma_1}, \end{aligned} \quad (77)$$

where we assumed the upstream and downstream incoherent scattering to be purely Gaussian, and  $dw_{\text{cont}}$  is the angular distribution function in a pure continuous potential (slightly averaged over the particle incidence angles). The small portion of multiple Coulomb scattering within the arbitrarily isolated volume reflection region may be included *either* in the upstream *or* downstream scattering

piece, as long as it is small, and thus additive. Moreover, if in (77) we change the integration variables, one integration can be taken, with the result

$$\frac{dw}{d\chi} = \int d\alpha \frac{dw_{\text{cont}}(\alpha)}{d\alpha} \times \frac{1}{\sqrt{2\pi(\sigma_1^2 + \sigma_2^2)}} e^{-\{[(\theta-\alpha)^2]/2[(\sigma_1^2 + \sigma_2^2)]\}} \quad (78)$$

depending only on the sum  $\sigma_1^2 + \sigma_2^2$ . Obviously, the latter sum must be equated to  $\sigma_{\text{am}}^2(L + \Delta L)$ , and thereby the precise positions of the boundaries separating the different kinetic regions prove to be inessential. Neglecting  $\Delta L$  compared to  $L$  in the argument of  $\sigma_{\text{am}}$  amounts to the approximation of [8].

In practice, usually, the width of  $dw_{\text{cont}}/d\alpha$  is smaller than  $\sigma_{\text{am}}^2$ , whereby the resulting angular distribution becomes close to a Gaussian, anyway. Therefore, it is described essentially in terms of the first two moments:

$$\langle \chi \rangle = \int d\chi \chi \frac{dw}{d\chi} \quad \left( \int d\chi \frac{dw}{d\chi} = 1 \right), \quad (79)$$

and

$$\sigma^2 = \int d\chi (\chi - \langle \chi \rangle)^2 \frac{dw}{d\chi}. \quad (80)$$

The mean value  $\langle \chi \rangle$  only receives a contribution from  $dw_{\text{cont}}/d\chi$ :

$$\langle \chi \rangle = \int d\chi \chi \frac{dw_{\text{cont}}}{d\chi} \quad (81)$$

(as was implied in Sec. III), while when we evaluate  $\sigma^2$  from Eq. (78), the coherent and incoherent contributions to it appear to be just additive:

$$\begin{aligned} \sigma^2 &= \sigma_{\text{am}}^2(L + \Delta L) + \sigma_{\text{cont}}^2 \\ &\equiv \sigma_{\text{am}}^2(L) + \sigma_{\text{am}}^2(R\langle \chi \rangle) + \sigma_{\text{cont}}^2, \end{aligned} \quad (82)$$

with

$$\sigma_{\text{cont}}^2 \equiv \int d\chi (\chi - \langle \chi \rangle)^2 \frac{dw_{\text{cont}}}{d\chi}. \quad (83)$$

Angular distribution  $dw_{\text{cont}}/d\chi$  has some differences, for positive and negative particles [9], as does the nuclear interaction rate calculated in Sec. II. Let us begin with the case of positive particles, to which most of the data refer.

### 1. Positively charged particles

For positive particles, at  $R > 4R_c$ ,  $\sigma_{\text{cont}}$  was quoted in (11). For a realistic continuous potential the numerical coefficient in Eq. (11) may slightly differ, but that is not crucial for the following estimates.

Measurements of total  $\sigma^2$  for 400 GeV protons interacting with a (110) silicon crystal were carried out in experiment [32]. There, in order to get access to the intrinsic volume reflection angular divergence  $\sigma_{\text{cont}}$ , the difference

$$\sigma^2 - \sigma_{\text{am}}^2(L) = \bar{\sigma}_{\text{v.r.}}^2 \quad (84)$$

was evaluated. From Eq. (82) we see, however, that it differs from pure  $\sigma_{\text{cont}}$ :

$$\begin{aligned} \bar{\sigma}_{\text{v.r.}} &= \sqrt{\sigma^2 - \sigma_{\text{am}}^2} = \sqrt{\sigma_{\text{cont}}^2 + \sigma_{\text{am}}^2(R\langle \chi \rangle)}, \\ \bar{\sigma}_{\text{v.r.}} &\neq \sigma_{\text{cont}}. \end{aligned} \quad (85)$$

Assuming condition (63a) to hold, we may insert explicit theoretical expressions (62), (11), and (10) into Eq. (85), which leads to a nonscaling  $R$  dependence of the measured quantity  $\bar{\sigma}_{\text{v.r.}}$ :

$$\bar{\sigma}_{\text{v.r.}} = \sqrt{\frac{\pi^2}{12\theta_c^2} \frac{d^2}{R^2} + \frac{\pi\theta_c}{2} \left( \frac{11 \text{ MeV}}{E} \right)^2 \frac{R - d/\theta_c^2}{X_0}}. \quad (86)$$

The most characteristic feature of function (86) is the existence of a minimum. The minimum location is found by equating to zero the derivative of the radicand with respect to  $R$ :

$$R_*(E) = \frac{1}{\theta_c} \sqrt[3]{\frac{\pi}{3} X_0 d^2} \left( \frac{E}{11 \text{ MeV}} \right)^{2/3} \simeq \left( \frac{E}{38 \text{ GeV}} \right)^{7/6} [\text{m}]. \quad (87)$$

The physical meaning of  $R_*$  is not drastically different from that of  $R_{\text{mult}}$ —it marks the scale of  $R$  where the multiple scattering compares with coherent deflection angles, with the proviso that  $R_{\text{mult}}$  is derived from generic reasoning in terms of the particle trajectory, while  $R_*$  in terms of specific contributions to the beam broadening in the crystal. However, the actual expressions for  $R_{\text{mult}}$  and  $R_*$  are not equivalent; moreover, their ratio

$$\frac{R_{\text{mult}}}{R_*} = \left( \frac{3}{\pi} \frac{E}{11 \text{ MeV}} \right)^{1/3} \left( \frac{X_0}{d} \right)^{1/6} \sqrt{\frac{\theta_c}{2}} \simeq \left( \frac{E}{50 \text{ MeV}} \right)^{1/12} \quad (88)$$

depends on the particle energy, albeit pretty weakly. At ultrarelativistic energies, ratio (88) is  $>1.5$ , justifying the use of Eq. (86), but up to LHC energies it does not exceed 3. The value of  $\bar{\sigma}_{\text{v.r.}}$  at the minimum equals

$$\bar{\sigma}_{\text{min}} = \bar{\sigma}_{\text{v.r.}}(R = R_*) \simeq \left( \frac{1 \text{ keV}}{E} \right)^{2/3}. \quad (89)$$

The available data at  $E = 400 \text{ GeV}$  (presented in Fig. 5) reach beyond  $R_*$ , which according to Eq. (87) amounts to

$$R_*(400 \text{ GeV}) \approx 16 \text{ m}. \quad (90)$$

Around  $R_*$ , the data show a flattening of the  $R$  dependence. However, the point at  $R = 35.71 \text{ m}$ , which exceeds  $R_u$ , resumes the decrease of  $\bar{\sigma}_{\text{v.r.}}$ , and departs from our

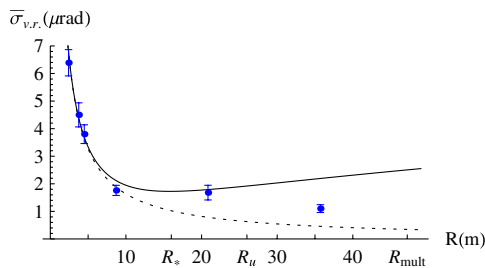


FIG. 5. Subtracted final beam angular width vs the crystal bending radius, for  $E = 400$  GeV protons in a  $L = 2$  mm silicon crystal. Solid curve—theoretical prediction [Eq. (86)]. Dotted curve—pure  $\sigma_{\text{cont}}$  (also compatible with calculation of [8] in a more realistic continuous potential model). Points—experimental data [32].

theoretical prediction. Although in that domain our equations are no longer valid, qualitatively the decrease of  $\bar{\sigma}_{v,r}$  may be understood from the point that as the relative variation of  $\dot{r}$  within the nuclear region increases,  $\dot{r}$  in this region on average gets larger than in the middle of the plane, and so the total nuclear interaction probability diminishes.

## 2. Negatively charged particles

For negative particles, the experimental data are too scarce to extract the  $\bar{\sigma}_{v,r}^2(R)$  behavior, so we restrict ourselves to delineating the main theoretical anticipations.

First of all, for negatively charged particles the expression for  $\sigma_{\text{cont}}(R)$  somewhat differs, though its  $R$  dependence keeps close to  $1/R$ , up to logarithmic factors. Second, in this case we have  $\Delta\sigma_{\text{am}}^2 \propto \langle \Delta L \rangle < 0$ . Therefore, the expression for  $\bar{\sigma}_{v,r}^2$  for negative particles is similar to the radicand of Eq. (86), but with a negative coefficient at the second term. That implies that for negative particles  $\bar{\sigma}_{v,r}^2$  changes sign and becomes *negative* for sufficiently large  $R$ . That is the salient feature of the final beam angular distribution for negative particles, which is apt for experimental verification.

Next, since  $\sigma_{\text{cont}}$  for positively and for negatively charged particles differ, in general it is not as straightforward to compare the angular broadenings for positive and negative particles, as it was for the rate of inelastic nuclear interactions. However, in the region  $R > R_*$  where  $\sigma_{\text{cont}}$  gets relatively small, that must already be feasible. The simplest way of pinning down  $\sigma_{\text{cont}}$ , though, is to measure both angular beam divergence components perpendicular and parallel to the family of the active atomic planes.

## V. SUMMARY

The problem of multiple Coulomb scattering at volume reflection belongs to the category of combined potential and stochastic motion, and is complicated even in the radial 1D case. However, in the limit of small multiple scattering angles, relevant at most of the experimental realizations of volume reflection, we proved a quite simple

relation according to which the difference between the probability of any kind of nuclear interaction of a proton in a bent crystal and in an amorphous target is proportional to the particle mean volume reflection angle and the crystal bending radius [Eqs. (17) and (44), and a similar Eq. (49) for negative particles]. These relations exploit only the local character of nuclear interactions and the periodicity of atomic planes in the crystal, and do not resort to any parametrization for the continuous potential, such as the parabolic approximation used in our earlier treatment of volume reflection [9].

We also examined the physical conditions of applicability of our equations in the case of positive particles. It resulted in introducing two scales for the crystal bending radius as functions of the particle energy. First,  $R_u(E)$  [Eq. (56)], is the radius at which the width of distribution of atomic nuclei in atomic planes becomes relevant. The second,  $R_{\text{mult}}(E)$  [Eq. (64)], is where the multiple Coulomb scattering affects the plane-crossing angles near the volume reflection point. We had also estimated the probability of volume capture under conditions typical for volume reflection. At high energies, it is small, but the process is interesting in its own right. Although its  $E$  and  $R$  dependences comply with the predictions of previous authors, the temperature dependence thereof appears to be different. The estimates provided and scales introduced are expected to be of rather general significance for the volume reflection and volume capture processes.

The perturbative prediction for positive particles was confronted with the experimental data [14,32], both for the rate of inelastic nuclear interactions and for the angular divergence of the volume-reflected beam. The theoretical predictions are in a satisfactory agreement with the experimental data.

As we mentioned in the Introduction, monitoring of the nuclear interaction excess (either by inelastic nuclear interaction events, or through the measurement of the final beam angular divergence) may potentially be used for *in situ* diagnostics of the quality of volume reflection-based crystalline deflector. The information received from incoherent interactions in the crystal is complementary to that obtained from measurements of coherent processes, such as coherent bremsstrahlung in a bent crystal [33,34].

In conclusion, we remind that our study is concerned only with the volume part of the effect. Under conditions when either  $R$  grows, or  $L$  decreases, so that  $R\theta_c$  becomes comparable to  $L$ , there must also arise boundary effects, in the same manner as for the volume reflection angle itself [35]. In contrast, volume capture probability, even at large  $R$ , should be less sensitive to boundary effects.

## ACKNOWLEDGMENTS

The author thanks V. Guidi, A. V. Shchagin, and A. M. Taratin for reading the manuscript and useful comments.

- [1] A. M. Taratin and S. A. Vorobiev, *Phys. Lett. A* **119**, 425 (1987); *Nucl. Instrum. Methods Phys. Res., Sect. B* **26**, 512 (1987).
- [2] Yu. M. Ivanov *et al.*, *Phys. Rev. Lett.* **97**, 144801 (2006).
- [3] Yu. M. Ivanov *et al.*, *JETP Lett.* **84**, 372 (2006).
- [4] W. Scandale *et al.*, *Phys. Rev. Lett.* **98**, 154801 (2007); *Phys. Rev. ST Accel. Beams* **11**, 063501 (2008).
- [5] S. Hasan *et al.*, *Nucl. Instrum. Methods Phys. Res., Sect. B* **269**, 612 (2011).
- [6] W. Scandale *et al.*, *Phys. Rev. Lett.* **102**, 084801 (2009).
- [7] V. Tikhomirov, *Phys. Lett. B* **655**, 217 (2007); W. Scandale *et al.*, *Phys. Lett. B* **682**, 274 (2009); W. Scandale *et al.*, *Europhys. Lett.* **93**, 56002 (2011).
- [8] V. A. Maishev, *Phys. Rev. ST Accel. Beams* **10**, 084701 (2007).
- [9] M. V. Bondarenco, *Phys. Rev. A* **82**, 042902 (2010).
- [10] W. Scandale *et al.*, *JINST* **6**, T10002 (2011).
- [11] Processes of close interaction with atomic nuclei also include atomic K-shell ionization, with the accompanying characteristic x-ray (CXR) radiation, occurring at fast charged particle passage close to the nucleus. However, CXR has attenuation length  $\sim 10 \mu\text{m}$ , which is generally too small compared with the thickness of crystals applied for volume reflection.
- [12] V. M. Biryukov, V. N. Chepegin, Yu. A. Chesnokov, V. Guidi, and W. Scandale, *Nucl. Instrum. Methods Phys. Res., Sect. B* **234**, 23 (2005); A. M. Taratin and W. Scandale, *ibid.* **262**, 340 (2007).
- [13] A. M. Taratin, *Phys. Part. Nucl.* **29**, 437 (1998).
- [14] W. Scandale *et al.*, *Nucl. Instrum. Methods Phys. Res., Sect. B* **268**, 2655 (2010).
- [15] M. V. Bondarenco, *Phys. Lett. A* **376**, 875 (2012).
- [16] Working with ultrarelativistic particles, we adopt the system of units in which the speed of light  $c = 1$ .
- [17] E. N. Tsyganov, Fermilab Report No. TM-682, 1976; Fermilab Report No. TM-684, 1976.
- [18] V. M. Biryukov, Yu. A. Chesnokov, and V. I. Kotov, *Crystal Channeling and its Application at High-Energy Accelerators* (Springer, Berlin, 1996).
- [19] In [8], where this parameter was originally introduced, it was designated as  $\kappa$ .
- [20] In paper [9] the final beam angular distribution was described in terms of  $d\lambda/d\theta$ , the differential cross section. But obviously, dividing that quantity by  $d$ , we obtain the normalized probability distribution  $\frac{dw_{\text{cont}}}{d\theta} = \frac{1}{d} \frac{d\lambda}{d\theta}$ ,  $\int d\theta \frac{dw_{\text{cont}}}{d\theta} = 1$  handled in the present paper.
- [21] It may be noted that all the high-energy nuclear and electromagnetic cross sections are weakly energy dependent. In addition,  $n_{\text{at}}$  has a weak dependence on the crystal temperature.
- [22] In this article, it will be convenient to choose the angle counting direction so that volume reflection angles (opposite in sign to the crystal bending direction) are positive.
- [23] I. S. Gradshteyn and I. M. Ryzhik, *Tables of Integrals, Series and Products* (Academic Press, San Diego, 1980), 5th ed.; T. M. Apostol, *Introduction to Analytic Number Theory* (Springer, New York, 1976).
- [24] F. W. J. Olver, *Asymptotics and Special Functions* (Academic Press, New York, 1974).
- [25] A more consistent derivation of  $\langle(\delta X)^2\rangle$  in terms of the Debye temperature [36] gives analytically different but numerically close relation.
- [26] C. Flensburg and R. F. Stewart, *Phys. Rev. B* **60**, 284 (1999).
- [27] G. R. Lynch and O. I. Dahl, *Nucl. Instrum. Methods Phys. Res., Sect. B* **58**, 6 (1991); V. L. Highland, *Nucl. Instrum. Methods* **129**, 497 (1975); **161**, 171 (1979); K. Nakamura *et al.* (Particle Data Group), *J. Phys. G* **37**, 075021 (2010).
- [28] This formula was derived from experiments with hadronic projectiles, elastic scattering of which on nuclei also includes contribution from strong interaction. But for simplicity, in the literature the whole process is called multiple Coulomb scattering, or just multiple scattering.
- [29] M. L. Ter-Mikaelian, *High-Energy Electromagnetic Processes in Condensed Media* (Wiley, New York, 1972).
- [30] V. Biryukov, *Phys. Lett. A* **205**, 340 (1995).
- [31] V. M. Biryukov and S. Bellucci, *Nucl. Instrum. Methods Phys. Res., Sect. B* **266**, 235 (2008); V. M. Biryukov, *ibid.* **267**, 2457 (2009).
- [32] W. Scandale *et al.*, *Phys. Rev. Lett.* **101**, 234801 (2008).
- [33] W. Scandale *et al.*, *Phys. Rev. A* **79**, 012903 (2009).
- [34] Yu. A. Chesnokov, V. I. Kotov, V. A. Maishev, and I. A. Yazynin, *JINST* **3**, P02005 (2008); A. G. Afonin *et al.*, *JETP Lett.* **88**, 414 (2008); W. Scandale *et al.*, *Phys. Rev. A* **79**, 012903 (2009); M. V. Bondarenco, *Phys. Rev. A* **81**, 052903 (2010); Yu. A. Chesnokov, V. A. Maishev, D. Bolognini, S. Hasan, M. Prest, and E. Vallazza, *Phys. Rev. ST Accel. Beams* **13**, 070706 (2010).
- [35] M. V. Bondarenco, *Nuovo Cimento Soc. Ital. Fis. C* **34**, 381 (2011); arXiv:1103.0770.
- [36] H. Uberall, *Phys. Rev.* **103**, 1055 (1956); L. I. Schiff, *ibid.* **117**, 1394 (1960).